Preparation and Properties of Poly(Ethylene Terephthalate)/ATO Nanocomposites

Xiaolei Chen, Chunzhong Li, Wei Shao, Junqing He

Key Laboratory for Ultrafine Materials of Ministry of Education, School of Materials Science and Engineering, East China University of Science and Technology, Shanghai 200237, People's Republic of China

Received 23 February 2007; accepted 10 March 2007
DOI 10.1002/app.26511
Published online 15 May 2007 in Wiley InterScience (www.interscience.wiley.com).

ABSTRACT: Antimony doped tin oxide (ATO) nanoparticles modified poly(ethylene terephthalate) (PET) composites used for manufacturing antistatic PET fiber were synthesized by *in situ* polymerization. The crystallization and multiple melting behavior of the nanocomposites were systemically investigated by means of Differential Scanning Calorimeter (DSC), Fourier Transform Infrared (FTIR), X-ray Diffraction (XRD) techniques. The degree of crystallinity in nanocomposites increased with increasing ATO content. Smaller and more incomplete crystals are presented in the crystalline regions of the nanocomposites with increasing the content of ATO, which could be attributed to heterogeneous nucleation effects of ATO nanoparticles. Dynamic Mechanical Analysis (DMA) measurements showed that the storage moduli of the nanocomposites increased with increasing the content of ATO, due to formation of immobilized layer between polymer and filler. The interactions between ATO and PET molecules result in high tan δ for the PET/ATO nanocomposites. Percolation threshold of PET/ATO hybrid fibers prepared by the nanocomposites at room temperature was as low as 1.05 wt %, much lower than that of the composites filled with conventional conductive particles. Adding ATO nanoparticles obviously improves the conductivity of PET. © 2007 Wiley Periodicals, Inc. J Appl Polym Sci 105: 2783–2790, 2007

Key words: poly(ethylene terephthalate); nanocomposites; *in situ* polymerization; antimony doped tin oxide; crystallization

INTRODUCTION

Organic/inorganic nanocomposites comprise one of the most important classes of synthetic engineering materials.[1–5] Several methods including solution polymerization, melt polymerization, emulsion polymerization, and *in situ* polymerization,[6–11] have been used to obtain polymer nanocomposites. Poly(ethylene terephthalate) (PET) is a material with low cost and high performance, which has been found wide applications in fiber and nonfiber fields. However, the high specific resistance (more than 10^{14} Ω cm) and the static problem of PET will restrict its further application. At present, the antistatic PET nanocomposites were prepared mostly by adding conducting nanoparticles and the incorporation can result in materials possessing permanent antistatic property.[12,13]

Antimony doped tin oxide (ATO) exhibits both optical transparency to visible radiation and high electrical conductivity. ATO has been intensively studied for its high-temperature, chemical and mechanical stabilities.[14] At low antimony (Sb) doping level, the conductivity of ATO is greatly increased as compared to pure tin oxide and can be varied easily by changing the Sb doping level.[15] When used as antistatic agent, ATO shows better performance than the currently used carbon blacks, metallic pigment and organic polymer binders.[16] A novel fabric finishing agent containing ATO nanoparticles has been prepared and used for antistatic treatment for PET fabric.[17] The surface resistance of PET fabric treated by the novel finishing agent could be decreased from order of 10^{12} Ω to 10^{10} Ω.

In this article, an *in situ* polymerization method was established for preparing PET/ATO antistatic nanocomposites. The effects of ATO loading on the crystallization behavior, the dynamic mechanical properties of PET/ATO nanocomposites, and electrical property of the PET/ATO hybrid fibers were investigated.

EXPERIMENTAL

Materials

ATO nanoparticles were prepared by chemical coprecipitation method, which had been described previously.[18] Its characteristics were listed in Table I. Ethylene glycol (EG), cobalt acetate (as catalyst), antimony trioxide (as catalyst), and terephthalic acid

Correspondence to: C. Li (czli@ecust.edu.cn).

TABLE I
Characteristics of the ATO Sample

Sample	BET surface area ($m^2\ g^{-1}$)	Average particle size (nm)	Volume resistivity (Ω cm)
ATO	65	20	$1 \sim 5$

(TPA) were kindly supplied by Shanghai Chemical Fiber Institute.

Preparation of PET/ATO nanocomposites

The PET/ATO nanocomposites were synthesized in 2 L reactor fabricated by Shanghai Chemical Fiber Institute. ATO nanoparticles were modified by silane coupling agent and dispersed in EG by ball-milling at 25°C. Since the synthetic procedures for all nanocomposites were almost the same, only a representative example, the procedure for the preparing nanocomposites containing 1.0 wt % ATO, is described here. A mixture of 403 g of EG (with 12.7 g of modified ATO), 830 g of PTA, 0.017 g of cobalt acetate, and 0.248 g of antimony trioxide was placed into a 2 L reactor. The mixture was first agitated at a rate of 30 rpm at room temperature. The mixture was then quickly heated to 255°C to esterify it in nitrogen atmosphere and under a pressure of 1.5×10^5 Pa. During the esterification, the pressure was slowly reduced to atmospheric pressure to emit the water generated. Afterward, the polymerization was carried on at $270 \sim 280$°C, and the pressure of polymerization was gradually reduced to 70 Pa using suction. A power meter was used to denote the polymerization level. When the power meter increases to 50%, for each sample, the polymerization time has little difference (with variation from 120 to 150 min), the agitation was stopped. Finally, the melting polymer was extruded through an orifice at a N_2 pressure of 1.5 kg and then cooled with water. The neat PET and nanocomposites at a different ATO content were fabricated by the same process. A mixed solvent of phenol/1,1,2,2-tetrachloroethane (TCE) was used for the measurement of solution viscosity. The product was dried under a vacuum at 80°C for 24 h before viscosity measurement. The solution viscosity numbers (listed in Table II) range from 0.645 to 0.725.

Spinning

The products were dried in vacuum for 48 h at 120°C prior to spinning. The neat PET and nanocomposites at a different ATO content were spun into fiber with 36 monofilaments on an ABE-25 spinning machine at a speed of 1200 m/min; the temperatures in the screw region are listed in Table III. Then the drawing of fiber was carried out on a Barmag3013 drawing device at a temperature of 160°C with a draw ratio of 3.8.

Characterization

The fractured surface morphologies of PET/ATO nanocomposite were investigated by Scanning Electron Microscope (SEM) (JEOL JSM-6360LV, Japan). An SPI sputter coater was used to sputter-coat the fractured surfaces with gold to enhance conductivity.

The neat PET and nanocomposites at a different ATO content were sectioned into 90 nm thick slices by an ultramicrotome (Model Reichert-fung) and placed on a mesh 200 copper net. The photographs of ultrathin sections of the samples were characterized using Transmission Electron Microscope (TEM) (Model JEM-2010).

The thermal behavior was studied by Differential Scanning Calorimeter (DSC) (Model Netzsch PC200). The temperature of the instrument was calibrated with indium. All tests were performed under a stream of nitrogen gas. For each measurement, the samples were performed at two heating cycles. The first heating cycle was that the samples were heated to 300°C and kept for 10 min in the hermetic cell to remove the thermal history. The second heating cycle was that the samples were cooled at 10°C/min to 100°C and reheated at 10°C/min to 280°C to study the crystallization and melting of the PET/ATO nanocomposites. Both crystallization and melting parameters were obtained from cooling and heating scans.

The crystal structures of PET/ATO nanocomposites were analyzed by X-Ray Diffraction (XRD) (Model D/MAX-2550PC) at room temperature with Cu K_α radiation ($\lambda = 0.154056$ nm). The generator was operated at a voltage of 40 kV and a generator current of 100 mA. Testing data were collected from 1.5 to 40° at a scanning rate of 5°/min. The samples

TABLE II
The Properties of Neat PET and PET/ATO Nanocomposites

ATO (wt %)	0	0.5	1.0	2.5	5.0
η_{inh}[a]	0.645	0.675	0.685	0.710	0.725

[a] Inherent viscosities were measured at 30°C by using 0.1 g/100 mL solutions in a phenol/1,1,2,2-tertachloroethane (w/w) mixture.

TABLE III
Spinning Technical Parameters of PET/ATO Nanocomposites

	Screw					
Section no.	1	2	3	4	Spinning pump	Spinning beam
Temperature (°C)	287	305	300	300	300	310

were cut using dicing cutter at room temperature after polymerization and had no thermal history.

The crystallinity measurement by XRD is based on the Vainshtein intensity conservation law. The total intensity of diffraction is the summation of intensity both in crystalline region and in amorphous region; thus the crystallinity of fiber is calculated as follows:[19]

$$X_c = \frac{\int_0^\infty S^2 I_c(s) ds}{\int_0^\infty S^2 I(s) ds} \quad (1)$$

where X_c is the crystallinity of neat PET and PET/ATO nanocomposites; $S = 2\sin\theta/\lambda$; I(s) is the total intensity of diffraction; I_c(s) is the intensity of diffraction in crystalline region.

Infrared spectra of neat PET and the nanocomposites were recorded with a Nicolet Avatar 360 ATR-FTIR instrument (Nicolet Instrument, USA). Each sample was scanned 100 times at a resolution of 2 cm^{-1} from 1200 to 800 cm^{-1}.

The dynamic mechanical properties of the samples were studied with DMA equipment (Model IDMA2890). The samples were analyzed in the three-point bending mode. These properties were measured at 1 Hz, in the temperature range between 15 and 250°C with a heating rate of 4°C/min. The samples were vacuum dried for 5 h at 90°C before they are molded. The samples for DMA testing were prepared by pressing PET chips to a rectangular flat-plate in a flat-plate vulcanizing machine at 260°C and 15 MPa for 3 min. After this period, the rectangular flat-plate, containing the nanocomposites, was rapidly cooled to room temperature by cold press at 10 MPa for 10 min. The nanocomposites at a different ATO content were prepared by the same process.

Two parameters were used to study the glass transition of neat PET and PET/ATO nanocomposites. The glass transition temperature (T_g) can be defined as the maximum of the transition in the loss tangent curve. The full-width at half-maximum (FWHM) (see Fig. 1 for a scheme of the criteria used to define this parameter) refers to the homogeneity of the amorphous phase, so that a bigger FWHM value implies a higher inhomogeneity of the amorphous phase.

The electrical properties of the fibers were measured with the specific resistance tester (Model YG321) at 25°C. An average of at least 10 individual determinations was obtained.

RESULTS AND DISCUSSION

Morphology of PET/ATO nanocomposites

The dispersion of ATO nanoparticles in the PET matrix was crosschecked by using electron microscope data. Dispersion and morphology of ATO nanoparticles were examined using SEM images. SEM images of 2.5 wt % ATO in PET are shown in Figure 2. Figure 2 shows that ATO agglomerates still exist, but their size is less than 200 nm. The ATO agglomerates are well dispersed in the polymer matrix. Inorganic nanoparticles are difficult to disperse in polymer matrix because of particle agglomeration and immiscibility between the inorganic particles and the polymer matrix. Therefore it is suggested that the modification method of ATO by silane coupling agent and using EG as a media of mixture in a ball-milling mixing could provide better dispersion of ATO in PET. PET/ATO nanocomposites were prepared by means of esterification and condensation reactions of TPA and EG with modified ATO nanoparticles.

The interface structure between ATO and PET matrix was studied by TEM. Typical TEM photographs for PET/ATO nanocomposite at a different ATO content were shown in Figure 3. Figure 3 shows ATO particles were bonded tightly to PET matrix in the form of loose conglomerates. The loose conglomerates are more easily form conducting network structure. Figure 3 also shows that agglomerated structures become denser in the PET matrix with

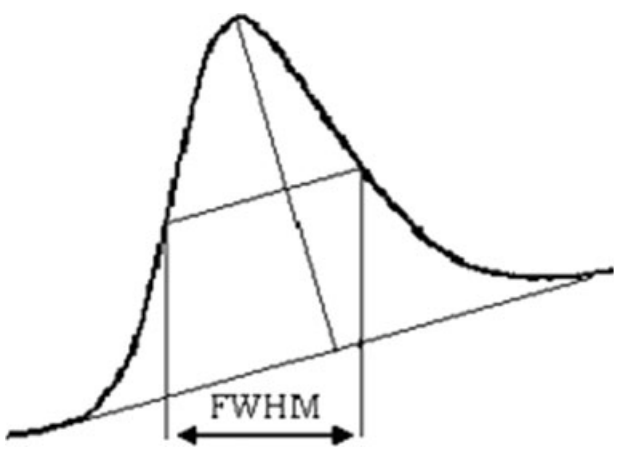

Figure 1 Criteria of definition of the parameter FWHM.

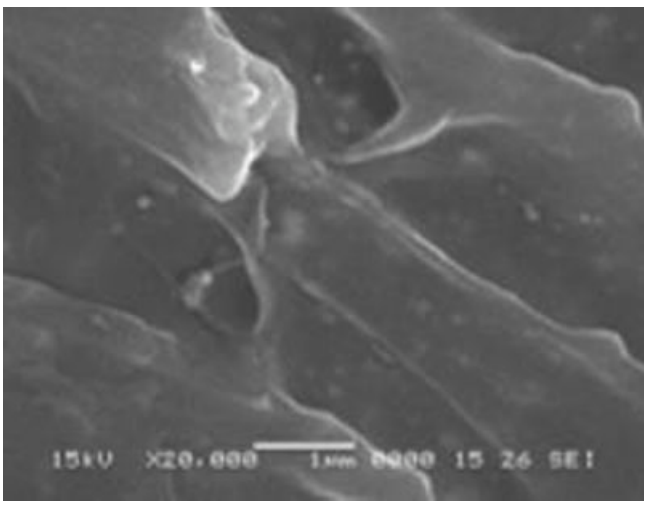

Figure 2 SEM micrographs of PET/ATO nanocomposites.

increasing ATO content. This result indicates that higher concentration of filler (more than 2.5 wt %) is not beneficial for dispersing nanoparticles in polymer matrix.

Crystallization and thermal behavior of PET/ATO nanocomposites

Rong et al.[20] have shown that the addition of silica nanoparticles have no significant effect on the crystallization process and the crystallization temperature of polypropylene (PP). However, other scientists[21–24] have reported that adding particles increased the crystallization rate of polymer. In this study, it was found that adding ATO nanoparticles resulted in a change in the thermal properties of PET. Figure 4 shows the cooling curves of neat PET and PET/ATO nanocomposites. It is evident that there is a distinct exothermic crystallization peak in all of the cooling scans, and the peak is symmetrical. It can be seen that at the cooling rate of 10°C/min, the crystallization exothermal peak is gradually shifted to high temperature with increasing content of ATO. The half-peak width is narrowed as the ATO content is increased. The DSC thermograms recorded during the cooling of the samples from melt with a constant cooling rate and showed a prominent crystallization exothermic peak. When the crystallization exothermic peak is symmetrical, the half crystallization time ($t_{1/2}$) can be obtained from this equation:

$$t_{1/2} = (T_{on} - T_c)/\chi \quad (2)$$

where T_{on} is the crystallization onset temperature, which is the temperature where the thermograph initially departs from the baseline, T_c is the temperature where the exotherm shows a peak, and χ is the cooling rate (°C/min).

The results for $t_{1/2}$ and the thermal dynamics parameters of the cooling process for PET/ATO nanocomposites were summarized in Table IV. The crystallization temperature T_c values for PET/ATO nanocomposites were higher than those of neat PET. The 97.5/2.5 PET/ATO exhibits the highest T_c value (198°C) of the PET/ATO nanocomposites. Changes in the crystallization peak width (ΔT_c) and the crystallization enthalpy (ΔH_c) are related to the overall

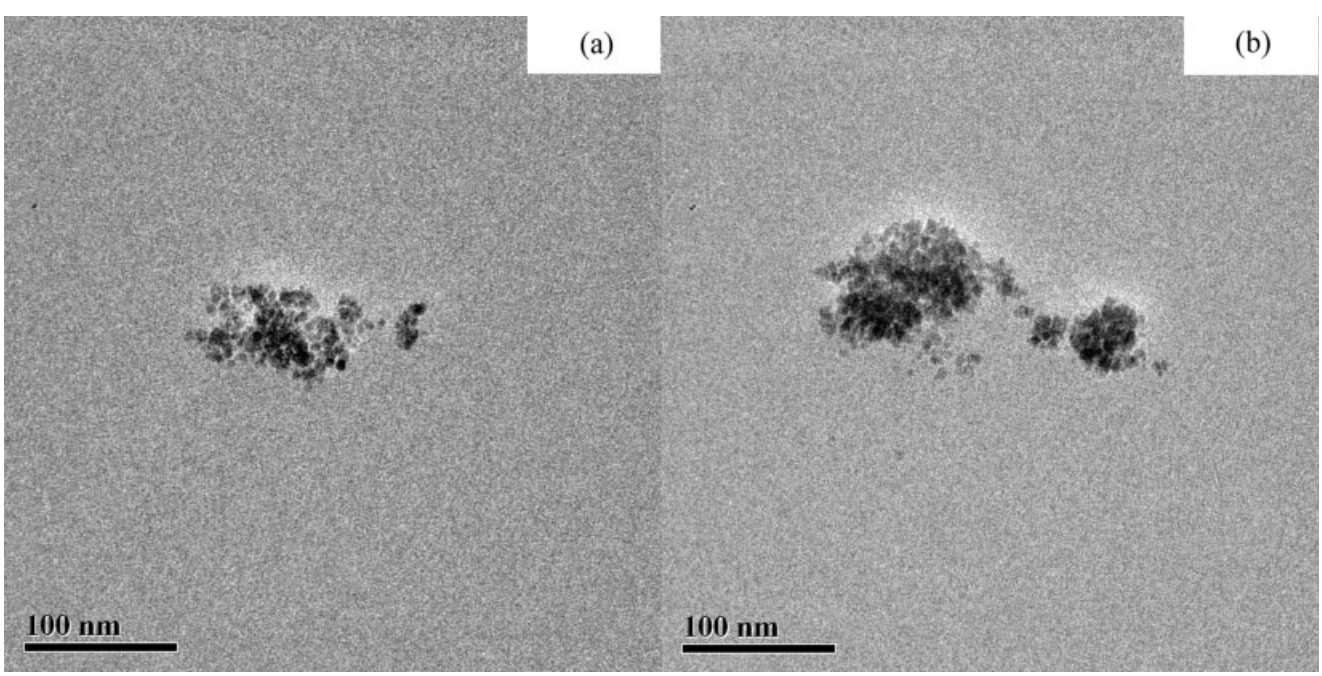

Figure 3 TEM micrographs of PET/ATO nanocomposites. (a) PET/ATO: 99/1 (b) PET/ATO: 97.5/2.5.

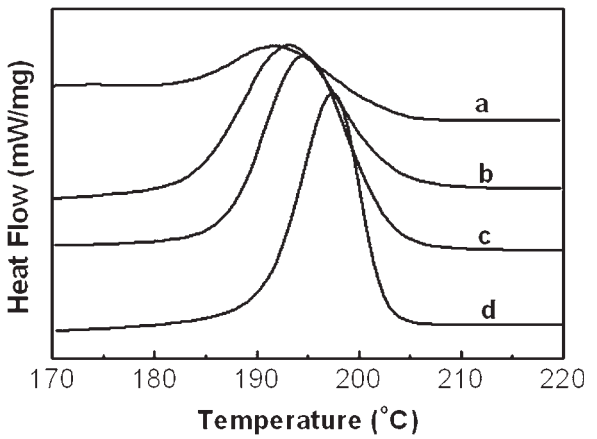

Figure 4 Cooling measurement of DSC trace for (a) neat PET (b) PET/ATO: 99.5/0.5 (c) PET/ATO: 99/1 (d) PET/ATO: 97.5/2.5.

crystallization rate and the extent of crystallization, respectively. The ΔT_c values for the blends are narrower by 2–14°C than that of neat PET (30°C) and the 97.5/2.5 PET/ATO exhibit the narrowest ΔT_c (16°C). The $t_{1/2}$ values of the nanocomposites are smaller than that of neat PET. The 97.5/2.5 PET/ATO exhibit the smallest $t_{1/2}$ (0.8 min), and their crystallization rates are nearly 2.0 times that of neat PET. From the data listed in the Table IV, the values of ΔH_c for all blends increase with increasing the ATO content. The 97.5/2.5 PET/ATO exhibits the largest ΔH_c value (40.8 J/g).[25]

It is generally known that the degree of supercooling ($\Delta T^c = T_m - T_c$), can be used to characterize the crystallization behavior of polymer. The degree of supercooling may be a measurement of a polymer's crystallizability; that is, the smaller the ΔT^c, the higher the overall crystallization rate. The ΔT^c values of the PET/ATO specimens are given in Table IV. The ΔT^c values of the PET/ATO nanocomposites are smaller, by 2–6°C, than that of neat PET (60°C), and the 97.5/2.5 PET/ATO exhibits the smallest ΔT^c.

From these results in Table IV, it is evident that the crystallization rate of PET phase in PET/ATO nanocomposite is increased due to the introduction of ATO nanoparticles. It can be explained that ATO exhibits a strong heterophase nucleation effect on PET crystallization due to its enormous surface area. The result is similar to both systems of nylon1212/MMT28[26] and PET/TiO_2.[23] These results indicate that ATO may be an ideal nucleating agent for PET processing.

Figure 5 depicts the heating runs of neat PET and PET/ATO nanocomposites. There is an endothermic melting peak on all of the heating scans. The symbols and resulting data of samples are listed in Table IV. No obvious changes in T_m values as ATO loading increased. The melting peak width (ΔT_m) is related to the thermal stability and the distribution of crystallites. A clear increase (8–12°C) in ΔT_m is found in the nanocomposites with respect to neat PET (61°C). In other words, the distribution of crystallites of PET in PET/ATO nanocomposites is broader than that of neat PET. The values of ΔH_f for all nanocomposites are larger than that of neat PET (30.5 J/g). This reveals that the amount (degree) of crystallinity of PET increases with the addition of ATO nanoparticles.

Figure 5 shows that increasing ATO loading in PET systems two melting exotherm peaks were observed. It is obvious that an additional melting peak appears at a lower temperature $T_{m,1}$ (243°C) in nanocomposites, and the area of the peak increases with increasing the ATO content, whereas the area of the peak at ~253°C ($T_{m,2}$) decreases. In general, the explanation for the appearance of multiple peaks in polymer melting curves[27–30] (such as nylon-6) is that the heat released by the reorganization of imperfect crystals to more perfect or stable crystals counteracts the heat absorbed during melting. We suggest that such an explanation is also suitable for our system. Upon heating, for neat PET the crystals formed (from the noncrystalline population) are finally melted at a higher temperature ($T_{m,2}$), together with those crystals formed during the first cooling process. Since the thermal history is identical for all of the neat and nanocomposite samples, in view of the absence of $T_{m,1}$, it is suggested that the $T_{m,1}$ observed in the nanocomposites probably originated from melting of the imperfect crystals induced by the existence of ATO, while the $T_{m,2}$ corresponds to the melting of the dominant crystals formed dur-

TABLE IV
DSC Data for PET/ATO Nanocomposites

Nanocomposite (PET/ATO)	Melting			Crystallization					
	T_m (°C)	ΔT_m (°C)	ΔH_m (J g^{-1})	T_{onset} (°C)	T_c (°C)	ΔT_c (°C)	$t_{1/2}$ (min)	ΔH_c (J g^{-1})	ΔT^c (°C)
100/0	252	61	30.5	207	192	30	1.5	35.7	60
99.5/0.5	252	69	32.5	208	194	28	1.4	37.5	58
99/1	253	69	33.6	207	195	24	1.2	38.9	58
97.5/2.5	252	73	32.3	206	198	16	0.8	40.8	54

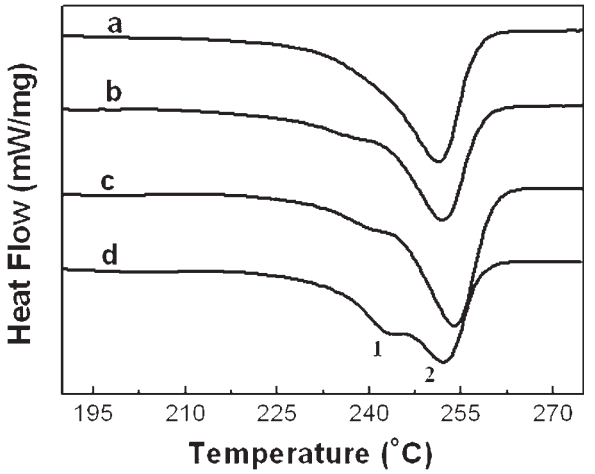

Figure 5 Heating measurement of DSC trace for (a) neat PET (b) PET/ATO: 99.5/0.5 (c) PET/ATO: 99/1 (d) PET/ATO: 97.5/2.5.

ing the first cooling process. With increasing the ATO content, there are more incomplete crystals in PET matrix and peak of $T_{m,1}$ becomes more obvious.

Crystalline structure and perfection

The XRD results for neat PET and the nanocomposites at a different ATO content are shown in Figure 6. Figure 6 shows that the diffraction peak of PET is more obvious with increasing the ATO content. The peak at $2\theta = 26.3^\circ$ is indexed as the (100) reflection plane. The reflection peak becomes sharper as the ATO increases, that is, the full-width at half-maximum of the (100) plane gradually decreases. According to Scherrer equation, the narrower diffraction peak shows the smaller sizes of crystallites in PET matrix. The crystallinity of neat PET and nanocomposites were calculated and are listed in Table V. It

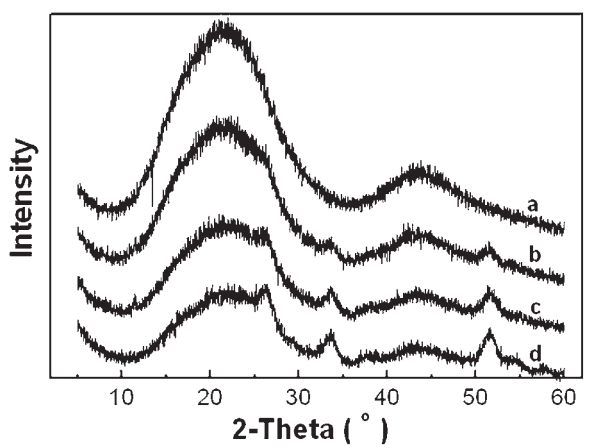

Figure 6 XRD patterns of PET and hybrid PET. (a) neat PET (b) PET/ATO: 99.5/0.5 (c) PET/ATO: 99/1 (d) PET/ATO: 97.5/2.5.

TABLE V
Data of the Crysyallinity for Neat PET and PET/ATO Nanocomposites

Samples (PET/ATO)	100/0	99.5/0.5	99/1	97.5/2.5
X_c (%)	16.88	22.70	25.09	33.30

could be seen that crystallinity increases with increasing the ATO content. By combining the XRD data with the DSC data, it can be easily understood that the ATO nanoparticles act as the nucleating agent in the PET crystallization process and accelerate the crystallization rates. Therefore smaller and more incomplete crystals formed in nanocomposites and ATO nanoparticles increased the crystallinity of PET.

To shed light on the lamellar structure of the nanocomposite, we used FTIR to identify trans and gauche conformations of ethylene glycol segments as shown in Figure 7. In the crystal regions, most of the ethylene glycol segments tend to adopt the trans conformation corresponding to absorption peaks at 974, 875, and 846 cm^{-1}, whereas in the amorphous region, the ethylene glycol segments may have the gauche conformation corresponding to absorption peaks at 1174 and 1041 cm^{-1}, especially in the interfacial region. Figure 7 shows that the relative intensity, which is the absorption peaks of the trans conformation versus that of the gauche conformation, increases from neat PET to PET/ATO (97.5/2.5) nanocomposite. This implies that more ethylene glycol segments may be present in the crystal region in nanocomposites comparing with neat PET. This may be attributed to the higher crystallinity of the PET/ATO (97.5/2.5) nanocomposite with adding the ATO.[31]

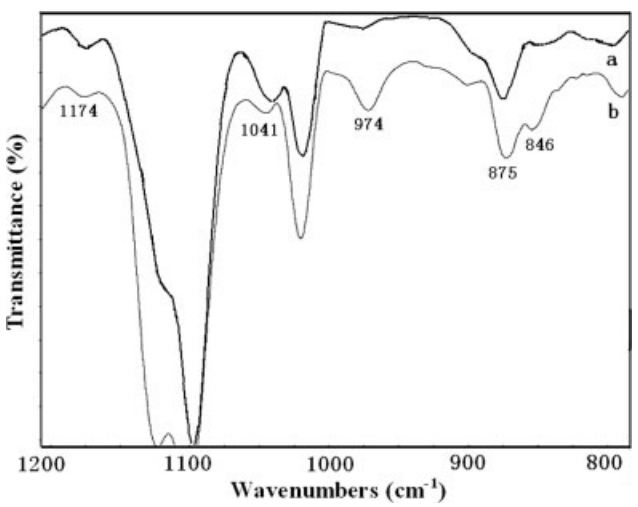

Figure 7 FTIR spectra of PET/ATO nanocomposites. (a) neat PET (b) PET/ATO: 97.5/2.5.

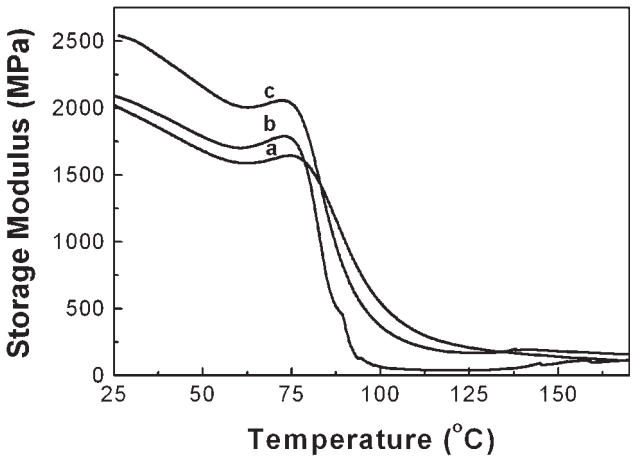

Figure 8 Storage modulus of the PET and hybrid PET. (a) neat PET (b) PET/ATO: 99/1 (c) PET/ATO: 97.5/2.5.

Dynamic mechanical properties

The storage modulus results of the neat PET and nanocomposites are shown in Figure 8. Figure 8 shows that:

$$E'(\text{PET/ATO: 97.5/2.5}) > E'(\text{PET/ATO: 99/1}) > E'(\text{neat PET})$$

The storage modulus always increases with increasing the content of ATO. This is the result of forming immobilized layer between polymer and filler. Besides, the crystallinity of PET increased with increasing the content of ATO. So, the PET/ATO nanocomposites have a higher storage modulus than the neat PET.

The DMA tan δ curves are shown in Figure 9. It can be seen that the tan δ always increases with

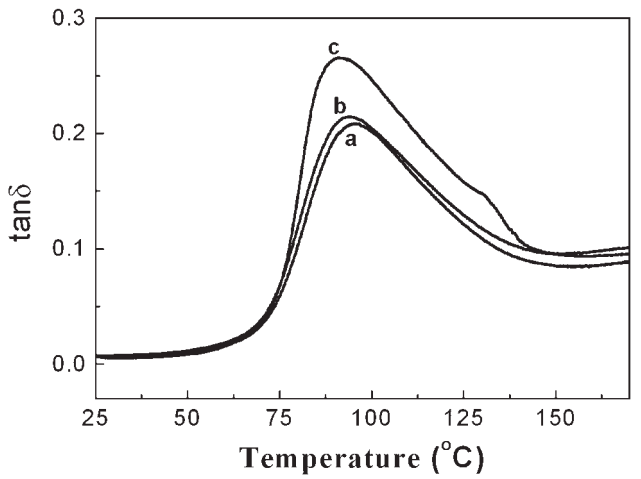

Figure 9 Loss tangent of the PET and hybrid PET. (a) neat PET (b) PET/ATO: 99/1 (c) PET/ATO: 97.5/2.5.

TABLE VI
Values of T_g and FWHM for Neat PET and PET/ATO Nanocomposites

Samples (PET/ATO)	T_g (°C)	FWHM
100/0	94.6	36
99/1	93.0	39
97.5/2.5	90.1	43

increasing the content of ATO. For the PET/ATO nanocomposite, ATO nanoparticles have extremely large surface areas; interactions between ATO and PET molecules are expected to be intensive. These intensive molecular-level interactions may be the major reason to result in high tan δ for the PET/ATO nanocomposites. According to the Figure 9, the results of T_g were included in Table VI:

$$T_g(\text{neat PET}) > T_g(\text{PET/ATO: 99/1}) > T_g(\text{PET/ATO: 97.5/2.5})$$

The experimental results prove that the T_g of PET/ATO nanocomposites occurs at lower temperatures. This might be explained with the aid of the DSC results: the ATO acts as a nucleating agent, and this effect of the ATO leads to a higher nucleation density and a faster crystallization of the PET. This higher nucleation density and faster crystallization cause an increase of the interface zone between crystalline phase and amorphous phase in the PET/ATO nanocomposites and results in an increase of the free volume. The higher the free volume, the more space for molecular mobility. Therefore need lower energy to rotate molecular segments and result in lower the T_g value. Similar experimental result was report for the polypropylene-talc composites.[32]

According to the Figure 9, the results of FWHM values were included in Table VI:

$$\text{FWHM(PET/ATO: 97.5/2.5)} > \text{FWHM(PET/ATO: 99/1)} > \text{FHWM(neat PET)}$$

This can be explained that the nucleating effect of the ATO, which makes the crystallization of the PET/ATO nanocomposites faster, so the amorphous zone is more inhomogeneous in nanocomposites than in the neat PET.

Electrical property

Variations of the electrical conductivities of neat PET and the PET/ATO hybrid fibers with different ATO content are shown in Figure 10. The resistances (R) of the hybrid fibers were measured by specific resistance tester and the specific resistances (ρ_v) of the hybrid fibers were obtained from R, using the relation:

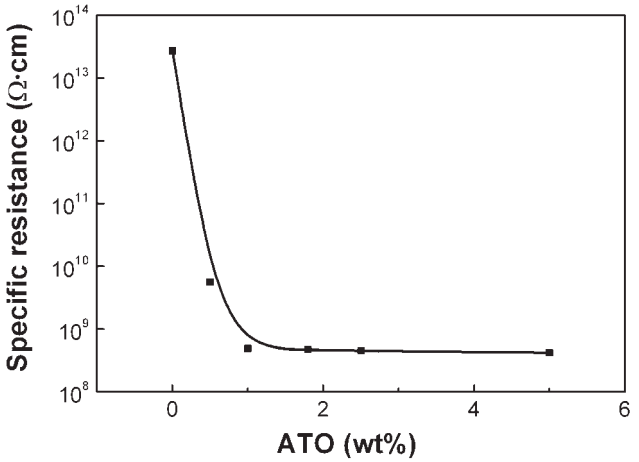

Figure 10 Effect of ATO contents on the specific resistance of the hybrid fibers.

$$\rho_v = 12R \cdot f \quad (3)$$

where f is the standard filling degree of the fiber. f is 0.23 for the PET fiber.

Figure 10 shows that when ATO was increased from 0 to 5 wt % in hybrid fibers, the electrical properties of the fibers improved from 2.7×10^{13} to 4.5×10^{8} Ω cm, indicating that adding ATO nanoparticles obviously improved conductivity of PET. The other feature of interest in Figure 10 is that for PET/ATO hybrid fibers, an abrupt conductivity transition occurs at a critical ATO content, which can be designated as the percolation threshold. The fibers containing ATO nanoparticles exhibited a percolation threshold about 1.05 wt %; whereas the composites filled by other conductive powder possessed a much higher threshold concentration.[33] The advantage of ATO over conventional conductive powder is significant. This was consistent with the observation in Figures 2 and 3. ATO is not in form of single particle dispersing in PET matrix, but in the form of loose aggregates. The loose aggregates are uniformly dispersed in PET matrix. These loose aggregates are chain structure composed of several ATO particles, and more easily prone to form conductive network.[34]

CONCLUSIONS

PET/ATO nanocomposites were successfully fabricated by *in situ* polymerization. The effects of ATO on the crystallization and multiple melting behavior of PET and its nanocomposites have been comparatively investigated in detail. The results obtained indicate that the presence of ATO enhances the crystallinity of PET by acting as a heterogeneous nucleation agent, also makes the melting behavior much more complex. ATO nanoparticles enhance the crystallization rate of PET, and lead to the decrease of the crystallite size of PET. The storage modulus of PET increases and the T_g value of PET decreases with adding ATO. The fibers containing ATO nanoparticles exhibited a percolation threshold about 1.05 wt %. Adding ATO nanoparticles obviously improves the conductivity of PET.

The author wishes to thanks to the National Natural Science Foundation of China, the Shanghai Municipal Science and Technology Commission.

References

1. Giannelis, E. P. Adv Mater 1996, 8, 29.
2. Messersmith, P. B.; Giannelis, E. P. Chem Mater 1993, 5, 1064.
3. Pinnavaia, T. J. Science 1983, 220, 365.
4. Gilman, J. W. Appl Clay Sci 1999, 15, 31.
5. Chang, J. H.; Park, K. M. Polym Eng Sci 2001, 41, 2226.
6. Vaia, R. A.; Ishii, H.; Giannelis, E. P. Adv Mater 1996, 8, 29.
7. Vaia, R. A.; Jandt, K. D.; Kramer, E. J; Giannelis, E. P. Macromolecules 1995, 28, 8080.
8. Sun, S. S.; Li, C. Z.; Zhang, L.; Du, H. L.; Gray, B. Polym Intern 2006, 55, 158.
9. Zhang, L.; Chen X. H.; Li, C. Z. J Mater Sci 2005, 40, 2097.
10. Zhang, L.; Li, C. Z.; Huang, R. J Polym Sci Part B 2005, 43, 1113.
11. Zhang, L.; Li, C. Z.; Huang, R. J Polym Sci Part B 2004, 42, 1656.
12. Gao, G. Y.; An, S. L.; Yu, J. L. J Tianjin Polytech Univ 2005, 24, 12.
13. Huang, Y.; Li, Z. F.; Luo, G. H. China Syn Fiber Ind 2004, 27, 1.
14. Rajpure, K. Y.; Kusumade, M. N.; Suallart, M. N. N. N. Mater Chem Phys 2000, 64, 184.
15. Kim, K. H.; Lee, S. W.; Shin, D. W.; Park, C. G. J Am Ceram Soc 1994, 77, 915.
16. Orel, Z. C.; Orel, B.; Hodoscek, M.; Kaucic, V. J Mater Sci 1992, 27, 313.
17. Wu, Y.; Chi Y. B.; Ni, J. X. J Funct Polym 2002, 15, 43.
18. Qing, C. Y.; Luo, M. F.; Gu, H. C. J East China Univ Sci Technol 2001, 27, 261.
19. Ren, X.; Meng, J. Synth Technol Appl 1998, 13, 1.
20. Rong, M. Z.; Zhang, M. Q.; Zheng, Y. X.; Zeng, H. M.; Walter, R.; Friedrich, K. Polymer 2001, 42, 3301.
21. Cho, J. W.; Paul, D. R. Polymer 2001, 42, 1083.
22. Fu, X.; Qutubuddin, S. Polymer 2001, 42, 807.
23. Atsushi, T.; Miko, C. Polymer 2004, 45, 6647.
24. Chan, C. M.; Wu, J.; Li, J. X.; Cheung, Y. K. Polymer 2002, 43, 2981.
25. Cheng, F. O.; Mong, T. H.; Jia, R. L. J Appl Polym Sci 2003, 91, 140.
26. Wu, Z.; Zhou, C.; Zhu, N. Polym Test 2002, 21, 479.
27. Cebe, P.; Hong, S. D. Polymer 1986, 27, 1183.
28. Lu, X. F.; Hay, J. N. Polymer 2001, 42, 9423.
29. Kong, Y.; Hay, J. N. Polymer 2003, 44, 623.
30. Zheng, J. R.; Siegel, R. W.; Gregory, T. C. J Polym Sci Part B 2003, 41, 1033.
31. Wan, T.; Chen, L.; Chua, Y. C. J Appl Polym Sci 2004, 94, 1381.
32. Díez-Gutiérrez, S.; Rodríguez-Pérez, M. A.; De-Saja, J. A. Polymer 1999, 40, 5345.
33. Pinto, G.; Jimenez-Martin, A. Polym Compos 2001, 22, 65.
34. Zhang, Q. H.; Chen, D. J Polym Mater Sci Eng 2004, 20, 21.